

Earth Syst. Dynam., 8, 547–563, 2017  
<https://doi.org/10.5194/esd-8-547-2017>

© Author(s) 2017. This work is distributed under the Creative Commons Attribution 3.0 License.



# Emission metrics for quantifying regional climate impacts of aviation

Marianne T. Lund<sup>1</sup>, Borgar Aamaas<sup>1</sup>, Terje Berntsen<sup>1,2</sup>, Lisa Bock<sup>3</sup>, Ulrike Burkhardt<sup>3</sup>, Jan S. Fuglestedt<sup>1</sup>, and Keith P. Shine<sup>4</sup>

<sup>1</sup>CICERO, Center for International Climate Research, Oslo, Norway

<sup>2</sup>Department of Geosciences, University of Oslo, Oslo, Norway

<sup>3</sup>Deutsches Zentrum für Luft- und Raumfahrt, Institut für Physik der Atmosphäre, Oberpfaffenhofen, Germany

<sup>4</sup>Department of Meteorology, University of Reading, Reading, UK

Correspondence to: Marianne T. Lund ([m.t.lund@cicero.oslo.no](mailto:m.t.lund@cicero.oslo.no))

Received: 31 January 2017 – Discussion started: 7 February 2017

Revised: 11 May 2017 – Accepted: 11 May 2017 – Published: 10 July 2017

**Abstract.** This study examines the impacts of emissions from aviation in six source regions on global and regional temperatures. We consider the  $\text{NO}_x$ -induced impacts on ozone and methane, aerosols and contrail-cirrus formation and calculate the global and regional emission metrics global warming potential (GWP), global temperature change potential (GTP) and absolute regional temperature change potential (ARTP). The GWPs and GTPs vary by a factor of 2–4 between source regions. We find the highest aviation aerosol metric values for South Asian emissions, while contrail-cirrus metrics are higher for Europe and North America, where contrail formation is prevalent, and South America plus Africa, where the optical depth is large once contrails form. The ARTP illustrate important differences in the latitudinal patterns of radiative forcing (RF) and temperature response: the temperature response in a given latitude band can be considerably stronger than suggested by the RF in that band, also emphasizing the importance of large-scale circulation impacts. To place our metrics in context, we quantify temperature change in four broad latitude bands following 1 year of emissions from present-day aviation, including  $\text{CO}_2$ . Aviation over North America and Europe causes the largest net warming impact in all latitude bands, reflecting the higher air traffic activity in these regions. Contrail cirrus gives the largest warming contribution in the short term, but remain important at about 15 % of the  $\text{CO}_2$  impact in several regions even after 100 years. Our results also illustrate both the short- and long-term impacts of  $\text{CO}_2$ : while  $\text{CO}_2$  becomes dominant on longer timescales, it also gives a notable warming contribution already 20 years after the emission. Our emission metrics can be further used to estimate regional temperature change under alternative aviation emission scenarios. A first evaluation of the ARTP in the context of aviation suggests that further work to account for vertical sensitivities in the relationship between RF and temperature response would be valuable for further use of the concept.

## 1 Introduction

The global aviation sector has historically been one of most rapidly growing economic sectors, and the increase in activity is projected to continue in the foreseeable future. The impacts of aviation exhaust emissions on atmosphere and climate have been under scrutiny for several decades (e.g., Brasseur et al., 2016; Fahey et al., 1995; Lee et al., 2009; Penner et al., 1999; Sausen et al., 2005). Today, global avi-

ation contributes about 2 % of the total anthropogenic  $\text{CO}_2$  emissions. In addition to emissions of  $\text{CO}_2$ , aviation affects climate through a number of other mechanisms, including emissions of nitrogen oxides ( $\text{NO}_x$ ), aerosols and precursor species, aerosol–cloud interactions and formation of contrail cirrus. These have a much shorter lifetime than a perturbation to  $\text{CO}_2$  and hence produce distinctly inhomogeneous radiative forcing and contribute to further inhomogeneity in tem-

perature response. Moreover, the regional and global climate impact of equal emissions of short-lived species can vary depending on where, and even when, the emissions occur (e.g., Berntsen et al., 2006; Stevenson and Derwent, 2009). Knowledge of such spatial and temporal variability is important for understanding the climate impacts of the sector and can be an important consideration in mitigation.

The spatial variability – from emissions to impacts on atmosphere and radiative forcing to temperature response – that characterizes the aviation sector is well recognized in the scientific community. Several studies have explored the regional differences in aviation  $\text{NO}_x$ -induced ozone changes and quantified the radiative forcing (RF) of aviation emissions (Gilmore et al., 2013; Köhler et al., 2013; Lee et al., 2009; Olsen et al., 2013; Penner et al., 1999; Sausen et al., 2005; Stevenson and Derwent, 2009; Unger et al., 2013). However, fewer estimates of regional temperature response exist (Huszar et al., 2013; Jacobson et al., 2012; Olivie et al., 2012). Because of the lack of a one-to-one relationship between forcing and response patterns (Boer and Yu, 2003; Shindell et al., 2010), the strength of regional aviation-induced temperature changes cannot be inferred directly from the corresponding RF distributions. The only tools to provide temperature response and other climate variables on very detailed spatial scales (e.g., grid point level) are comprehensive climate or earth system models. However, most, if not all, individual economic sectors or individual mitigation measures cause small perturbations, making it difficult (or costly) to capture a robust signal of the consequent response in climate models without significantly scaling up the emissions. On the other hand, knowledge about contributions of individual sectors to total climate impact, and the effects of specific measures, is essential for the formulation and assessment of effective mitigation strategies.

Emission metrics, such as the global warming potential (GWP) and global temperature change potential (GTP), are tools which can serve as a bridge to policy making, and are commonly used for aggregating information and placing different emissions on a common scale. Several studies have also used simplified climate models to calculate the global-mean temperature response to aviation (Berntsen and Fuglestvedt, 2008; Khodayari et al., 2013; Lee et al., 2009; Marais et al., 2008; Skeie et al., 2009). While aggregation and synthesis is often necessary for reasons of applicability, any such spatially aggregated measure has the disadvantage that it hides the underlying spatial distributions of impacts and the strength of regional impacts.

Recent work has advanced the development of metric concepts which can capture regional impacts. Shine et al. (2005a) and Lund et al. (2012) explored the use of non-linear damage functions to capture spatial information about climate impacts in global metrics. Lund et al. (2012) compared the impact of  $\text{NO}_x$  and aerosol emissions from the transport sectors and found that the loss of information due to global averaging was largest in the case of aviation. How-

ever, currently the only metric to provide estimates of impacts on a sub-global scale is the absolute regional temperature change potential (ARTP) (Shindell and Faluvegi, 2009, 2010). The ARTP uses a set of regional climate sensitivities to provide time-varying surface temperature response in four latitude bands to emissions, accounting for the regional RF caused by the emissions. These sensitivities are derived from simulations with a coupled climate model and express the relationship between the pattern of a radiative forcing and the consequent surface temperature in a given latitude band. Hence, the ARTP provides additional insight into the geographical distribution of temperature change beyond that available from traditional global metrics. For instance, Collins et al. (2013) calculated ARTPs for emissions of short-lived climate forcers in four regions, while Lund et al. (2014) used the ARTP to quantify regional temperature impacts of on-road diesel emissions and Sand et al. (2016) examined Arctic temperature responses.

In this study we calculate GWP, GTP and ARTP for global and regional aviation emissions. We consider a broad set of forcing mechanisms and emissions in six separate source regions. Aviation-induced radiative forcing of ozone and aerosols are obtained from simulations with the chemistry-transport model OsloCTM3 (Søvde et al., 2012) and subsequent radiative transfer calculations, while the radiative forcing from the formation contrail cirrus is simulated with ECHAM5-CCMod (Bock and Burkhardt, 2016a, b). Based on this we calculate both global and regional emission metrics. This allows us to capture (i) the impact of regional aviation emissions on global temperature response and (ii) the regional temperature response to regional emissions. Using the ARTP, we then quantify the regional impact of the present-day (i.e., year 2006) aviation sector, showing the contributions over time from individual species and emission regions to the temperature response in different latitude bands. The set of regional climate sensitivities that form the basis for the ARTP, by expressing the inter-regional relationship between radiative forcings and temperature response, have so far only been derived by one climate model and for four broad latitude bands (Shindell and Faluvegi, 2009). Establishing such sensitivities requires a large number of multi-decadal simulations and is thus very costly in terms of computer resources. Taking our analysis one step further, we therefore compare the regional temperature response to aviation ozone and black carbon aerosols estimated using these regional climate sensitivities with results from simulations with three other climate models, hence performing a first evaluation of the application of the ARTP in the context of selected aviation forcing mechanisms.

## 2 Methodology

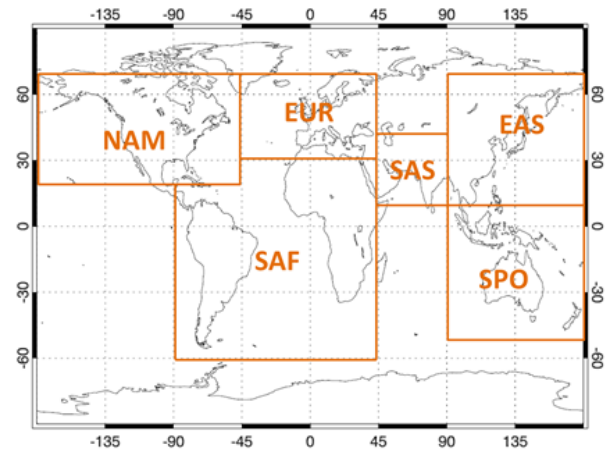
### 2.1 Atmospheric concentrations and radiative forcing

To quantify the changes in atmospheric concentrations of ozone and aerosols resulting from global and regional aviation emissions, the global chemistry-transport model OsloCTM3 is used (Søvde et al., 2012). The model is run with year 2010 meteorology and a T42 resolution (approximately  $2.8^\circ \times 2.8^\circ$ ) with 60 vertical layers from the surface to 0.1 hPa. Aviation emissions for 2006 are from the AEDT inventory (Wilkerson et al., 2010), while other anthropogenic and biomass burning emissions are from the HTAPv2 (Janssens-Maenhout et al., 2015) and Global Fire Emissions Database version 3 (GFED3; van der Werf et al., 2010) inventories. Guidance on how to access and use the AEDT emissions in atmospheric models is provided by Barrett et al. (2010). For input to the OsloCTM3, emissions are interpolated to the model's horizontal and vertical resolution, and averaged monthly. A 20 % perturbation of aviation emissions of black and organic carbon (BC, OC), sulfur dioxide (SO<sub>2</sub>) and NO<sub>x</sub> is applied globally and in six separate emission source regions, covering both hemispheres and the main flight corridors (Fig. 1): North America (NAM), Europe (EUR), East Asia (EAS), South Asia and Middle East (SAS), South America and Africa (SAF) and South Pacific Ocean (SPO). The impact of aviation is the differences between a baseline simulation with all emissions and each of the perturbations. Total aviation emissions by species and region are summarized in Table S1 in the Supplement.

As input to the emission metric calculations (Sect. 2.2), we calculate the global-mean RF for each emitted species  $i$  and emission region  $r$ , as well as the RF averaged over four latitude bands  $l$  (90–28° S, 28° S–28° N, 28–60 and 60–90° N) (RF <sub>$i,l,r$</sub> ). The direct forcing of aviation aerosols is quantified using the 3-D radiative forcing kernels developed by Samset and Myhre (2011), where the radiative forcing per burden was derived by imposing globally uniform perturbations of aerosol concentrations at 20 different pressure levels from the surface to 20 hPa. The NO<sub>x</sub>-induced ozone forcing is calculated using the Oslo radiative transfer model (RTM), including stratospheric temperature adjustment. The Oslo RTM consists of a broad band scheme for longwave radiation and a scheme using the multi-stream DISORT code for shortwave radiation (Myhre et al., 2000). The RF of NO<sub>x</sub>-induced methane changes is calculated as

$$\text{RF}_{\text{CH}_4,r} = \Delta\tau_{\text{CH}_4,r} \cdot [\text{CH}_4]_{2010} \cdot \text{RFeff}_{\text{CH}_4} \cdot f, \quad (1)$$

where  $\Delta\tau_{\text{CH}_4,r}$  is the relative change in methane lifetime between the control run and each of the emissions perturbations,  $[\text{CH}_4]_{2010}$  the 2010 global methane concentration of 1788 ppb,  $\text{RFeff}_{\text{CH}_4}$  the methane radiative efficiency of  $0.36 \text{ (mW m}^{-2}\text{) ppb}^{-1}$  (IPCC, 2014) and  $f$  the feedback factor of 1.34 (Holmes et al., 2013). The RF of the subsequent



NAM = North America, EUR = Europe, SAS = South Asia and Middle East, EAS = East Asia, SAF = South America and Africa, SPO = South Pacific Ocean

**Figure 1.** Definition of emission source regions in this study.

methane-induced ozone change – O<sub>3</sub> primary mode (PM) – (Wild et al., 2001) is calculated as

$$\text{RF}_{\text{O}_3\text{PM},r} = 0.5 \cdot \text{RF}_{\text{CH}_4}. \quad (2)$$

A decrease in atmospheric methane also results in a slight decrease in stratospheric water vapor, and hence an additional small negative RF, included in our RF<sub>CH<sub>4</sub></sub> based on Myhre et al. (2007) as

$$\text{RF}_{\text{SWV},r} = 0.15 \cdot \text{RF}_{\text{CH}_4}. \quad (3)$$

To obtain the latitudinal distributions RF<sub>CH<sub>4</sub>, $l,r$</sub>  and RF<sub>O<sub>3</sub>PM, $l,r$</sub>  we use the same approach as in Collins et al. (2013) and Lund et al. (2014) and scale results according to the latitudinal distribution of methane forcing derived from a global methane concentration perturbation (Fry et al., 2012).

In order to quantify the RF from the formation and persistence of contrail cirrus caused by global and regional aviation emissions, simulations with ECHAM5-CCMod (Bock and Burkhardt, 2016a, b) are performed at T42 resolution with 41 vertical levels using the same emission inventory and source regions as in the OsloCTM3. ECHAM5-CCMod is based on the ECHAM5-HAM (Lohmann et al., 2008), which is extended by a contrail-cirrus scheme with two-moment microphysics. The two-moment microphysical scheme allows for a more realistic representation of the microphysical and optical properties of contrail cirrus. The model is validated and used to provide updated calculations of stratosphere adjusted contrail-cirrus RF by Bock and Burkhardt (2016b), resulting in a global-mean RF of  $56 \text{ mW m}^{-2}$  for the 2006 AEDT aviation emissions used in this study. The existence of contrail cirrus results in a decrease in natural cirrus clouds, causing a negative RF that partly offsets contrail-cirrus warming. The magnitude of this

feedback effect is uncertain, but estimates suggest a forcing on the order of 20 % of the RF of contrail cirrus on global mean (Burkhardt and Kaercher, 2011). We include the feedback by reducing the contrail-cirrus RF by 20 % for all emission source regions, i.e., assuming, in the absence of more detailed information, that the negative RF is spatially constant.

The RFs are given by component, source region and latitude band in Table S2. Most of the species have short atmospheric lifetimes and consequently the RF is largest in the latitude bands closest to where the emissions occur. Some contrail-cirrus RF values are negative, which might be due to a change of cloud cover overlap in the model. There is a broad range in the estimates of global-mean RF caused by the various aviation emissions reported in the literature (e.g., Brasseur et al., 2016; Lee et al., 2009) and such uncertainties in RF will propagate to the emissions metrics. We therefore perform an uncertainty analysis as described in Sect. 2.2. Moreover, our results do not include effects of aerosol–cloud interactions, which is an important caveat. Studies suggest a potential impact of aviation BC on large scale cirrus clouds, but have yet to agree even on the sign of the radiative forcing (Zhou and Penner, 2014). A few studies have investigated effects of aviation emissions on liquid clouds, with global-mean RF estimates ranging from  $-46$  to  $-15 \text{ mW m}^{-2}$  (Gettelman and Chen, 2013; Kapadia et al., 2016; Righi et al., 2016), i.e., a negative RF that could offset a considerable fraction of the positive RF of contrail cirrus and ozone on a global scale. However, at present uncertainties in these estimates are also very large, and we consider that their inclusion here would be premature.

## 2.2 Global and regional emission metric calculations

We present calculations of the global and regional emission metrics GTP, GWP and ARTP for regional aviation emissions. The GWP and GTP methodology is extensively documented in the literature (e.g., Aamaas et al., 2013; Fuglestvedt et al., 2003; Shine et al., 2005b). Hence, we only describe the ARTP framework here.

The absolute regional temperature change potential (ARTP) gives the time-dependent temperature response following a pulse emission in the four latitude bands 90–28° S, 28° S–28° N, 28–60 and 60–90° N, accounting for the regional RF caused by the emissions. This regional temperature response is calculated using a set of regional climate sensitivities,  $\text{RCS}_{i,l,m}$ . The  $\text{RCS}_{i,l,m}$  is the unitless regional response in latitude band  $m$  due to a radiative forcing in latitude band  $l$  caused by a change in species  $i$ , relative to global sensitivity. Hence, the  $\text{RCS}_{i,l,m}$  express the relative regional response pattern. The regional climate sensitivities are developed based on a large set of simulations performed with the coupled atmosphere–ocean climate model GISS (Shindell and Faluvegi, 2009).

For BC, OC,  $\text{SO}_2$ ,  $\text{NO}_x$ -induced ozone and contrail cirrus, the ARTP in latitude band  $m$  at time  $H$  following a pulse emission is calculated as

$$\text{ARTP}_{i,r,m}(H) = \sum_l \frac{\text{RF}_{i,l,r}}{E_{i,r}} \cdot \text{RCS}_{i,l,m} \cdot \text{IRF}(H), \quad (4)$$

where  $\text{RF}_{i,l,r}$  is the RF in latitude band  $l$  caused by 1 year of emissions  $E_{i,r}$  of species  $i$  in region  $r$ . The impulse response function  $\text{IRF}(H)$  is a temporal temperature response to an instantaneous unit pulse of RF, which includes the global climate sensitivity. Here we have used the IRF of Boucher and Reddy (2008), which gives an equilibrium climate sensitivity (ECS) of  $1.06 \text{ K (W m}^{-2})^{-1}$ , equivalent to a 3.9 K equilibrium response to a doubling of  $\text{CO}_2$ . This is in the upper range reported in the Fifth IPCC Assessment Report (Bindoff et al., 2013). Assuming that the regional climate sensitivities scale linearly with the ECS, adopting a lower value reduces the magnitude of temperature response, and its time evolution, but does not affect the latitudinal distribution.

Equation (4) can be used for short-lived species where  $H$  is significantly longer than the lifetime of the species (typically days to weeks). In the case of  $\text{NO}_x$ -induced methane and subsequent ozone changes, the longer atmospheric residence time demands an additional IRF that describes the atmospheric decay of methane ( $\text{IRF}_{\text{long}}$ ). We add

$$\text{IRF}_{\text{long}}(t) = e^{-t/\tau}, \quad (5)$$

where  $\tau = 11.3$  years is the adjustment time for methane. The  $\text{ARTP}_{\text{long}}$  is then calculated following

$$\text{ARTP}_{i,r,m,\text{long}}(H) = \sum_l \int_0^H \frac{\text{RF}_{l,r}}{E_{i,r}} \cdot \text{IRF}_{\text{long}}(t) \cdot \text{RCS}_{i,l,m} \cdot \text{IRF}(H-t) dt. \quad (6)$$

The net ARTP is the sum of contributions given by Eqs. (4) and (6).

The  $\text{RCS}_{i,l,m}$  used in the emission metric calculations are summarized in Table S3. For OC, sulfate, nitrate, contrail cirrus and methane (plus methane-induced ozone changes) we use the  $\text{RCS}_{i,l,m}$  of the mean of the responses to  $\text{CO}_2$  and sulfate, as tabulated in Shindell and Faluvegi (2010). For BC and  $\text{NO}_x$ -induced ozone change the respective  $\text{RCS}_{i,l,m}$  from Shindell and Faluvegi (2009) (and tabulated in Collins et al., 2013) are used.

The temperature response per unit RF can differ between different forcing mechanisms, i.e., mechanisms can have their own specific climate sensitivity parameter. This is often expressed as an efficacy, defined as the ratio of the climate sensitivity parameter for a given forcing agent to that for a given change in  $\text{CO}_2$  (Hansen et al., 2005). The efficacy depends primarily on the spatial distribution of the RF, both in the horizontal and vertical. The  $\text{RCS}_{i,l,m}$  implicitly



include differences in efficacy of individual components arising from the horizontal forcing distribution (to the extent that the driving processes are accounted for in the underlying climate model simulations). The  $RCS_{i,l,m}$  are established for the four forcing agents BC, ozone, sulfate and  $CO_2$ . Contrail-specific regional sensitivities do not exist so far. Two studies have indicated that the efficacy of line-shaped contrails may be as low as 0.3–0.6 (Ponater et al., 2005; Rap et al., 2010). However, little or no information about the efficacy of contrail cirrus and the dependence of the climate sensitivity parameter of contrails on the horizontal forcing distribution exist. It should also be noted that efficacies from the small sector-specific forcings can currently only be derived by applying large scaling factors to produce RF of sufficient magnitude to give a significant response in the climate models. This adds an additional uncertainty to deriving reliable  $RCS_{i,l,m}$ , in particular for contrail cirrus due to the saturation effects. Using the average sensitivities of sulfate and  $CO_2$  to calculate the ARTPs of contrail cirrus allows us to account for a broader set of aviation-induced forcing mechanisms in our analysis, and these  $RCS_{i,l,m}$  include both a longwave absorption and a shortwave scattering component. The efficacy of scattering aerosols and greenhouse gases is also likely less dependent on altitude than for absorbing aerosols. However, we recognize that there can be uncertainties associated with this approach that can presently not be quantified. As for estimates of efficacies at the global scale, such as those given by Ponater et al. (2005) and Rap et al. (2010), these can be included in the metric application as a scaling factor, as discussed in Sect. 3.3. However, presently few studies have investigated the efficacy of aviation-induced forcing mechanisms. The dependence of the climate sensitivity parameter on the altitude of the perturbation is discussed in more detail in Sect. 3.4. We also explore potential uncertainties in our analysis arising from such vertical dependence by comparing the temperature responses estimated using the  $RCS_{i,l,m}$  with temperature simulated by three additional climate models (Sect. 2.3).

Emission metrics are given on a per unit emission basis. However, for contrail cirrus it is not clear how to pose the metric since no direct correspondence between an emission and the consequent forcing exists in this case. In order to provide consistent mass-based metrics for all components, we adopt the same approach as Fuglestedt et al. (2010) and calculate the contrail-cirrus GWP and GTP per unit  $CO_2$  emitted. However, as also discussed in Fuglestedt et al. (2010), an alternative is to relate the contrail-cirrus forcing to the distance flown. This approach may be more consistent with the way aircraft generate contrails and here we also provide metrics on a per kilometer basis. Both approaches are problematic when applying the methodology to future air traffic scenarios, which likely include fuel efficiency improvements. An increase in fuel efficiency causes a higher probability of contrail formation and at the same time a decrease in  $CO_2$  emissions. Therefore, contrail-cirrus RF per  $CO_2$  emission

would increase strongly, whereas contrail-cirrus RF per flight distance would increase less so.

In the following, we present emission metrics and calculate temperature changes for time horizons of 20 and 100 years after a 1-year pulse of present-day aviation emissions. Real-world emissions are of course not pulses but rather change over time following the development in economic activity, technology and regulations. However, pulse-based emission metrics can be used to quantify the net difference between two emission scenarios since any scenario can be viewed as a series of pulse emissions and analyzed through convolution (Eq. 7). Metrics for pulse emissions are also useful in themselves for illustrating the temporal behavior of various species. Realistic emissions will be continuous, leading to different relative contributions of short- and long-lived, warming and cooling species over time. Through the use of convolution, our metric framework can be used to estimate the temperature impact following any emission scenarios  $E_{i,r}(t)$ . For instance, the regional temperature response in latitude band  $m$  for species  $i$  for a scenario is the convolution of the emission scenario and the ARTP for a pulse emission (Aamaas et al., 2013):

$$\Delta T_{i,r,m}(t) = \int_0^t E_{i,r}(t') \cdot \text{ARTP}_{i,r,m} = (t - t') dt'. \quad (7)$$

For most short-lived species, the result will be a scaling of the ARTP value for a certain time horizon. However, this is not the case for  $NO_x$ , where the different timescales of the warming ozone effect and cooling effects linked to methane results in a change of the sign of the emission metric over time (as illustrated for GTP by Aamaas et al., 2016).

To establish ranges in the global-mean temperature change after 20 and 100 years due to uncertainties in RF and ECS, we perform a Monte Carlo analysis with 100 000 draws. Each RF mechanism is treated as a random variable, following a probability density function (PDF) defined based on existing literature. For the aerosols, we use the multi-model results from the AeroCom Phase II experiment (Myhre et al., 2013a), while for  $CO_2$  and the  $NO_x$ -induced changes in ozone and methane, we use the uncertainties from the IPCC AR5 (Myhre et al., 2013b). The  $NO_x$ -induced ozone and methane impacts are assumed to be dependent and a PDF for the net RF is established. Relative uncertainties are given in Table S4. For contrail cirrus we infer a lognormal distribution using the best estimate of  $0.05 \text{ W m}^{-2}$  and 90 % confidence interval of  $[0.02, 0.10] \text{ W m}^{-2}$  based on IPCC AR5. The distribution of the total RF is derived by summing the PDFs of individual mechanisms. This approach assumes that the forcing uncertainties are independent. We also adopt a lognormal distribution for the ECS and assume a best estimate of 3 K for a doubling of  $CO_2$ , and an upper and lower value of 1.5 and 4.5 K (Bindoff et al., 2013). Ranges are given at the 1 SD level (16th and 84th percentiles).

An additional source of uncertainty is the regional climate sensitivities. A full set of  $RCS_{i,l,m}$  have so far only been estimated with one climate model and it can be expected that they are likely model-dependent. When compared with the response to historical aerosol forcing in several other climate models, the sensitivities seem fairly robust (Shindell, 2012). Two studies have also repeated the BC experiments from Shindell and Faluvegi (2009) with similar findings in terms of spatial distribution of forcing and temperature response (Flanner, 2013; Sand et al., 2013). However, this evaluation is limited and a formal quantification of the uncertainty or model dependence is currently not possible.

### 2.3 Simulated temperature response

To evaluate the application of the ARTP in the context of aviation, we compare temperature responses estimated using the regional climate sensitivities from the GISS simulations with temperature response patterns simulated by three other climate models: the NCAR Community Earth System Model (CESM1.2) (Hurrell et al., 2013), HadSM3 (Williams et al., 2001) and ECHAM (Stenke et al., 2008). Simulations with the two latter models were performed within the EU project QUANTIFY (Ponater et al., 2009) and results used in Lund et al. (2012). Simulations with the CESM1.2 are performed for this study using the aviation ozone concentration perturbation from OsloCTM3. In order to obtain a statistically significant response to aviation ozone in the model, the perturbation is scaled by a factor of 40 (similar factors were applied in the HadSM3 and ECHAM simulations; see Lund et al., 2012, for details). We run a four-member ensemble of 60 years, using the last 30 in the analysis. The statistical significance is assessed using the false discovery rate (FDR) approach (Wilks, 2006). Here we focus on latitudinal patterns of temperature response, but we recognize that nonlinearities may arise when scaling of this magnitude is applied (e.g., Shine et al., 2012) and such uncertainties should be kept in mind when considering the absolute magnitude of temperature responses. Figure S1A in the Supplement shows the zonal annual-mean ozone concentration change caused by global aviation  $NO_x$  emissions from the OsloCTM3 (i.e., before scaling), while Fig. S1B shows the annual-mean CESM2.1 temperature response to the scaled ozone perturbation (hatching indicates statistical significance at the 0.05 level).

We also compare temperature responses to aviation BC simulated by HadSM3 using the same model configuration as given in Shine et al. (2012).

For comparison with climate model results, we use the regional climate sensitivities to estimate the regional equilibrium temperature response ( $\Delta T_{i,r,m}$ ) to a constant forcing following Eq. (6) of Shindell (2012),

$$\Delta T_{i,r,m} = \sum_l RF_{l,r} \cdot RCS_{i,l,m} \cdot ECS, \quad (8)$$

and adopting the equilibrium climate sensitivity (ECS) inherent in the IRF from Boucher and Reddy (2008) described above.

## 3 Results and discussion

### 3.1 Global emission metrics

Tables 1 and 2 summarize the 20- and 100-year GWPs and GTPs of global and regional aviation emissions, respectively, given relative to  $CO_2$  using the  $CO_2$  impulse response function ( $IRF_{CO_2}$ ) from Joos et al. (2013). The global GWPs and GTPs are not the main focus of our study but are included and briefly described for comparison with previous estimates. Our emission metrics do not account for climate-carbon feedbacks. If included, such feedbacks could increase the relative importance of non- $CO_2$  species (e.g., Gasser et al., 2017).

Our GWPs for the net effect of global aviation  $NO_x$  are somewhat higher than the range estimated by Skowron et al. (2013) using several different aviation emission inventories in a single model and Myhre et al. (2011) based on multi-model results (Table 1). They also fall in the upper end of the range reported by Fuglestad et al. (2010). The  $NO_x$  GTPs fall at or in the positive end of reported ranges. A number of factors can contribute to difference in the metric values, including differences in input radiative forcing, treatment and inclusion of methane-induced changes in ozone and stratospheric water vapor, and differences in the parameters of the  $IRF_{CO_2}$ . Our estimates also include the cooling effect from  $NO_x$ -induced formation of nitrate aerosols, which has to our knowledge not been accounted for in any previous aviation GWP and GTP estimates. The estimated contrail-cirrus GWPs and GTPs are similar to those given in Fuglestad et al. (2010). However, values are not directly comparable as we consider the combined RF of contrail cirrus (i.e., young line-shaped contrails and those cirrus originating from them, and their associated optical depth) and include the feedback of natural clouds in the present analysis. The RF of contrail cirrus was shown to be 9 times higher than the RF of line-shaped contrails when assuming constant optical depth (Burkhardt and Kaercher, 2011). Further differences arise from the use of different  $IRF_{CO_2}$ . Our GWPs and GTPs for BC and  $SO_2$  are higher than those derived by Fuglestad et al. (2010) by a factor of 2 and 4. However, the values from Fuglestad et al. (2010) are not specific for aviation emissions but based on input multi-model mean RF from all anthropogenic emissions (Schulz et al., 2006).

Quantifying the GTPs and GWPs of regional aviation emissions allows us to capture how equal emissions in different locations can have different impacts on the atmospheric concentrations and RF, and in turn on global climate. Our calculations reveal considerable differences between regions for all species, and both metrics and time horizons, with a factor of 2–4 (and higher for nitrate) difference between the

**Table 1.** GWP and GTP of global aviation emissions for time horizons of 20 and 100 years. Values are given on a per unit aviation emission basis (per kg BC, OC and SO<sub>2</sub>, respectively, with contrail cirrus calculated per kg aviation CO<sub>2</sub> and NO<sub>x</sub> per kg N). For comparison, aviation NO<sub>x</sub> GWP and GTP values from three previous studies are also included.

Component	GWP		GTP	
	<i>H</i> = 20	<i>H</i> = 100	<i>H</i> = 20	<i>H</i> = 100
Contrail cirrus	3.1	0.84	0.93	0.12
BC	3910	1060	1140	147
SO <sub>2</sub>	−559	−152	−162	−21
OC	−282	−77	−82	−11
NO <sub>x</sub>	411	77	−138	9
NO <sub>x</sub>				
Fuglesvedt et al. (2010)	120 to 470	−2.1 to 71	−590 to −200	−9.5 to 7.6
Myhre et al. (2011)	92 to 338	−21 to 67	−396 to −121	−5.8 to 7.9
Skowron et al. (2013)	142 to 332	4 to 60		

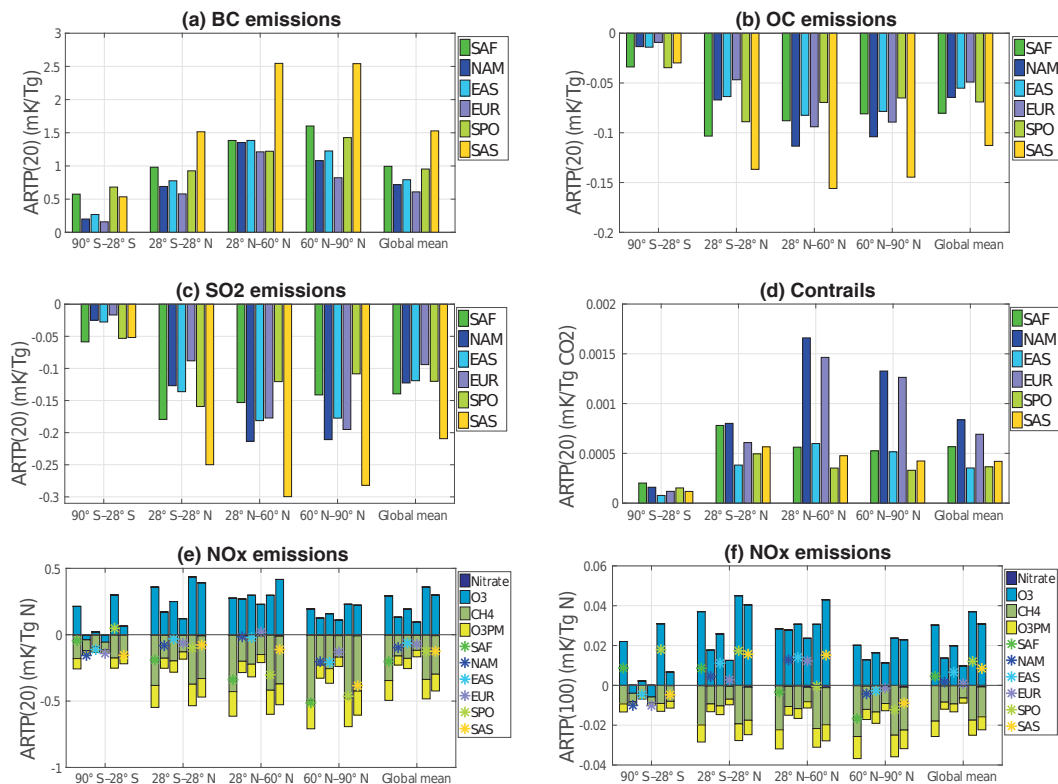


**Figure 2.** ARTP(20) of aviation (a) BC, (b) OC, (c) SO<sub>2</sub> and (d) contrail cirrus, and (e, f) ARTP(20) and ARTP(100) of aviation NO<sub>x</sub>. The asterisks in (e) and (f) show the net NO<sub>x</sub> effect of emissions in each source region, while the colored bars give the contributions from ozone production (O<sub>3</sub>), NO<sub>x</sub>-induced methane loss (CH<sub>4</sub>) (including subsequent stratospheric water vapor loss), methane-induced ozone changes (O<sub>3</sub> PM) and NO<sub>x</sub>-induced nitrate formation.

highest and lowest metric value (Table 2). For the aerosols we generally find the largest magnitude GWPs and GTPs for South Asia (SAS) emissions, followed by South America and Africa (SAF) or South Pacific Ocean (SPO). The high values for the SAS region reflects a relatively long lifetime of the aerosols here compared to other emission regions. This, in

turn, is likely driven by the underlying distribution of emissions, which is dominated by emissions at high altitudes (i.e., few flights landing or departing within the region), where conditions are drier (i.e., less wet scavenging of the aerosols). For NO<sub>x</sub>, the values are highest for SPO, while for contrail cirrus we find high values for aviation over NAM and EUR,

**Table 2.** GWP and GTP of regional aviation emissions for time horizons of 20 and 100 years. Values are given on a per unit aviation emission basis (per kg BC, OC and SO<sub>2</sub>, respectively, with contrail cirrus calculated per kg aviation CO<sub>2</sub> and NO<sub>x</sub> per kg N).

Component	Source region	GWP		GTP	
		<i>H</i> = 20	<i>H</i> = 100	<i>H</i> = 20	<i>H</i> = 100
Contrail cirrus	SAF	3.6	0.99	1.09	0.14
	NAM	3.3	0.90	1.00	0.13
	EAS	1.7	0.45	0.50	0.06
	EUR	2.5	0.67	0.75	0.10
	SPO	2.3	0.63	0.70	0.09
	SAS	2.6	0.70	0.78	0.10
BC	SAF	5420	1470	1570	203
	NAM	3560	969	1030	133
	EAS	4170	1140	1210	156
	EUR	2300	816	871	112
	SPO	4940	1340	1430	185
	SAS	8250	2250	2390	309
SO <sub>2</sub>	SAF	−833	−227	−242	−31
	NAM	−550	−150	−159	−21
	EAS	−602	−164	−175	−23
	EUR	−378	−103	−110	−14
	SPO	−746	−203	−216	−28
	SAS	−1120	−304	−324	−42
OC	SAF	−481	−131	−140	−18
	NAM	−289	−79	−84	−11
	EAS	−283	−77	−82	−11
	EUR	−197	−54	−57	−7.4
	SPO	−419	−114	−122	−16
	SAS	−611	−166	−177	−23
NO <sub>x</sub>	SAF	484	70	−316	6.26
	NAM	280	48	−126	5.0
	EAS	513	108	−79	13
	EUR	210	37	−87	4.0
	SPO	806	159	−205	19
	SAS	695	137	−176	16

where conditions for contrail formation are prevalent (e.g., Burkhardt et al., 2008; Irvine and Shine, 2015) and for SAF (see more detailed discussion in Sect. 3.2). From a policy perspective, knowledge of such regional differences is important if metrics are used to quantify the climate impact of emissions or emission changes in cases where there is a simultaneous change in the geographical emission distribution, or if used to evaluate the effect of implementing measures to reduce emissions in different regions.

While several studies have estimated GWPs and GTPs for global aviation NO<sub>x</sub> emissions, as discussed above, few have produced estimates for regional aviation emissions. Köhler et al. (2013) quantified the climate impact of aviation emissions in North America, Europe, India and China. The reported GWP(20) agrees within 10–30% with estimates for all regions in the present analysis, while our GTP(20) values are about 50% lower in absolute magnitude for all emission regions, and GWP(100) and GTP(100) for NAM and EUR are

50–100% higher than Köhler et al. (2013) estimates. Again it should be noted that these difference can be caused by a number of factors. Moreover, because the two studies use differently defined emission source regions, only a rough comparison is possible.

### 3.2 Regional emission metrics

While GWPs and GTPs illustrate how equal emissions in various regions can have different impacts on global climate, they can naturally not inform us of the actual regional distribution of impacts. The ARTP allows us to estimate temperature impacts with at least some spatial information.

Figure 2 shows the ARTP with a time horizon of 20 years (ARTP(20)) for BC, OC, SO<sub>2</sub> and contrail cirrus for each emission source region, and the ARTP(20) and ARTP(100) of aviation NO<sub>x</sub>. We do not show ARTP(100) for aerosols and contrail cirrus here. The absolute values decay strongly over time, but the latitudinal patterns will be identical on both time horizons. Results for global aviation emissions are given in the Supplement, as are contrail-cirrus metrics on a per kilometer basis.

For OC and SO<sub>2</sub> (Fig. 2b and c), we calculate the highest magnitude ARTP(20) (i.e., temperature impact per unit emission) for aviation in SAS in all latitude bands except 90–28° S, where values for SAF and SPO are slightly higher. Excluding the SAS region, aviation in EUR and NAM give the highest temperature impact per unit emission in the 28–60 and 60–90° N regions, which is also where the corresponding RF is strongest (Table S2). This is unsurprising given that these species are short-lived and the forcings they exert are largely localized to the emission region. However, using the ARTP reveals important differences between the latitudinal distribution of RF and subsequent temperature response. In given latitude bands, the temperature impact can be considerably stronger than the RF in that band suggests, and can extend to the opposite hemisphere to where the emissions occurred. This can be seen by comparing the latitudinal distribution of the RF values given in Table S2 with that of the ARTPs. Applying the  $RCS_{i,l,m}$  given in the coarse latitude bands smooths out the impacts such that there is less latitudinal variation in the temperature responses than in the RFs. This illustrates the dependence of temperature response on both forcing exerted locally and on remote impacts through large-scale circulation impacts and feedbacks in the climate system.

The latter effects are also very important in the case of BC (Fig. 2a). Again, the ARTP(20) is highest for aviation in SAS, while the difference between remaining regions is smaller than for OC and SO<sub>2</sub> in most latitude bands. In the 60–90° N region, aviation in the Southern Hemispheric regions cause the highest temperature per unit emissions, despite being far removed from the Arctic. In the GISS simulations, the Arctic temperature response to local (i.e., within Arctic) forcing is negative (Shindell and Faluvegi, 2009).



This local cooling effect applies to BC changes in the mid- to upper Arctic troposphere, which is where aviation is most important. Aviation BC emissions in EUR and NAM are more easily transported into the Arctic region and hence induce a stronger local forcing and in turn a larger surface cooling. The net effect of aviation in these regions on the Arctic is still a warming, but this warming is partly offset by the cooling contribution from within Arctic RF. In contrast, aviation BC emissions in SAS, EAS, SAF and SPO have less potential for long-range transport to the Arctic, but the remote BC forcing warms the Arctic through transport of energy. In terms of mitigation, these results underline that if the goal is to limit temperature increase, e.g., in the Arctic, it is necessary to go beyond radiative forcing as an indicator and to also consider the impact of emission in more remote regions. This feature has been illustrated also for other sectors and regions (Collins et al., 2013; Lund et al., 2014).

For contrail cirrus (Fig. 2d), the ARTP(20) for aviation in EUR and NAM is substantially larger in the 28–60 and 60–90° N latitude bands than for other source regions considered in this study, while the difference between source regions is less pronounced in the Southern Hemisphere latitude bands. There are two main competing processes at play. Contrail formation is generally more prevalent in the extratropics due to lower temperatures at flight levels than in the tropics and may persist longer due to larger probability of ice supersaturation. An upward shift in the flight level in the tropical troposphere increases the probability of contrails formation and ice supersaturation (Burkhardt et al., 2008). Local peaks of ice supersaturation are also found in the tropics (Irvine and Shine, 2015); in fact, the probability of ice supersaturation is highest in the upper tropical troposphere (Lamquin et al., 2012). Furthermore, once contrails have formed, the optical depth of contrail cirrus is higher in the tropics due to the larger amount of water vapor available for deposition. This higher optical depth in the tropics and the consequently higher RF has also been found in contrail-cirrus simulations (Burkhardt and Kaercher, 2011). However, none of our source regions cover only the tropics. In the SAS region, the air is mostly too warm for contrail formation. However, if contrails were present here, their radiative forcing efficiency would be high. Due to the competing short- and long-wave effects, there can be important diurnal and seasonal variability in the net impact of contrail cirrus (e.g., Stuber et al., 2006; Bock and Burkhardt, 2016b). The diurnal effects depend on assumptions about the contrail-cirrus lifetime and were shown to be small (Newinger and Burkhardt, 2012) when using the contrail-cirrus parameterization of Burkhardt and Kaercher (2011). This effect is not captured in our analysis using annual-mean RF as input.

It should be emphasized that the contrail-cirrus emission metrics are suitable for the average of the present-day aircraft fleet. Their application would not be appropriate if there are significant changes in routes and flight altitudes. Furthermore, future changes in climate may alter the meteorological

and dynamical conditions and hence affect the potential for contrail-cirrus formation in a given region (Irvine and Shine, 2015). As discussed in Sect. 2, several factors contribute to uncertainty in the emission metrics and should be kept in mind in further applications.

The ARTP of aviation NO<sub>x</sub> (Fig. 2e and f) is separated into contributions from ozone, methane and methane-induced ozone, as well as the direct effect of nitrate aerosols. The stars indicate the net NO<sub>x</sub> effect. The ARTP(20) is negative in all but two cases, i.e., the net effect of 1 year of aviation NO<sub>x</sub> emissions is a cooling on this timescale, dominated by the NO<sub>x</sub>-induced methane loss. However, it is important to note that the sign and magnitude of the net NO<sub>x</sub> effect is very sensitive to the choice of time horizon due to the very different timescales on which the ozone and methane contributions act. In particular, during the first decade after emission, the strong but short-lived warming from ozone dominates, resulting in a net positive effect (see also Fig. 6b of Fuglestad et al., 2010). Moreover, the NO<sub>x</sub> ARTP is also influenced by the spatial patterns of ozone and methane. Due to the shorter lifetime, the aviation-induced ozone perturbation is more heterogeneous than the methane concentration change, and more confined to the emission source region. The choice of time horizon may therefore affect both the net NO<sub>x</sub> effect and the relative importance of source regions. The impact of changes in both ozone and methane from a pulse emission on NO<sub>x</sub> decays strongly over time, as reflected by the much smaller ARTP(100). While the methane cooling remains important on longer timescales, the absolute magnitude diminishes strongly towards a time horizon of 100 years. For all source regions, the competing effects of ozone warming and methane cooling over time results in a small, but net positive global-mean effect of aviation NO<sub>x</sub> on a 100-year time horizon. In the 90–28° S latitude band the ARTP(100) is positive for emissions occurring in the Southern Hemisphere, but negative for emissions in the Northern Hemisphere, as the latter causes a much smaller ozone concentration change in this latitude band and the methane cooling becomes relatively more important over time. A similar response is seen in the 60–90° N latitude band.

### 3.3 Regional climate impacts of present-day aviation

To place our climate metrics in context and illustrate further application, we apply the ARTP and estimate the regional temperature responses over time to present-day aviation in the six emission source regions. Figure 3 shows the temperature change (net and contribution from each species) in each latitude band 20 and 100 years after a 1-year pulse of present-day aviation emissions in each source region. The current aviation climate mitigation policy is largely focused on CO<sub>2</sub>. The contributions from aviation CO<sub>2</sub> emissions are therefore added to place the impact of short-lived and long-lived species in context. The error bars show the 1 SD ranges due to uncertainties in RF and ECS (Sect. 2.2). Because the same

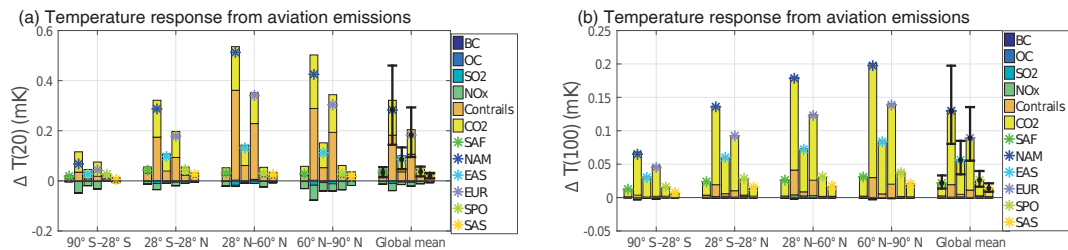


**Figure 3.** Regional and global-mean temperature change by species and source region after (a) 20 years and (b) 100 years following a 1-year pulse of emission from the present-day aviation sector in each source region. The asterisk shows the net temperature response in the respective latitude band for each emission source region, while the bars show the contribution from each species to the net. Error bars show the 1 SD ranges due to uncertainties in RF and ECS.

relative uncertainty is assumed for emissions in all source regions and our analysis does not account for uncertainty in the regional climate sensitivities, we only include the ranges in the global-mean temperature change.

The majority of flights today take place over the northern midlatitudes. As a result, the net warming is largest in all latitude bands for emissions over NAM and EUR. On a 20-year time horizon, the largest warming contribution from these source regions comes from contrail-cirrus formation and, despite the highly localized RF, the temperature impact is not only limited to the latitude band closest to where the emissions occur. The net warming is slightly offset by a small cooling due to  $\text{NO}_x$ -induced methane loss, especially in the 90–28° S and 60–90° N regions. As pointed out above, the sign and magnitude of the net  $\text{NO}_x$  effect depends strongly on the chosen time horizon. For instance, on a 10-year time horizon (not shown here), the net  $\text{NO}_x$  response is a warming in the 28° S–28° N and 28–60° N regions for emissions in NAM, EUR and EAS. Aviation emissions of BC are small and therefore contribute little to the net impact, despite the strong efficiency (i.e., temperature change per kg emitted).

Even on shorter time horizons (e.g., 20 years), the warming contribution from  $\text{CO}_2$  is important. For emissions in EAS, SAF, SAS and SPO,  $\text{CO}_2$  is of comparable magnitude to contrail cirrus after 20 years. On longer time horizons (e.g., 100 years) the  $\text{CO}_2$  contribution becomes dominant in all latitude bands. This has previously been illustrated for the global-mean temperature impact of the sector (Berntsen and Fuglestedt, 2008). Because the perturbation in  $\text{CO}_2$  is longer-lived and well mixed, the warming in the Southern Hemisphere becomes relatively more important compared to the other latitude bands on longer timescales. Nevertheless, for emissions in NAM and EUR, for the Northern Hemisphere response regions and the global mean, the contributions from contrail cirrus remain substantial and approximately 15 % of the  $\text{CO}_2$  response, even on these long timescales. Figure 3 also shows that the relative importance of the source regions across latitude bands following a pulse emission changes very little over time. However, these cal-

culations do not account for potential future changes in the geographical distribution of emissions.

The considerable uncertainty in the aviation-induced forcing mechanisms and climate sensitivity is reflected in the error bars. After 100 years, the uncertainty in climate sensitivity dominates as the relative contribution from the more uncertain but short-lived mechanisms decays and  $\text{CO}_2$  becomes more important. Note that the same relative uncertainties apply to all source regions. For contrail cirrus, an additional source of uncertainty is the efficacy. As noted in Sect. 2.2, studies indicate that the efficacy of contrail cirrus may be lower than one. Because only two estimates exist in the literature, efficacy is not included in present analysis. However, adopting a spatially uniform efficacy of, for example, 0.6 (Ponater et al., 2005) would result in a 40 % lower contrail-cirrus impact across all latitude bands.

Our study focuses on the pulse-based emission metrics and does not consider the future temperature impact of aviation following *emission scenarios*, which would change the timescale of the response and the relative importance of short- and long-lived species over time. As described in Sect. 2.2, our pulse-based emission metrics can be used in further studies to investigate the regional temperature impacts following more realistic emission scenarios. For instance, as the simplest form of scenario, one could assume that emissions are kept constant at the present-day level. In this case, the contributions from short-lived species such as contrail cirrus, ozone and sulfate would quickly become sustained at a constant level rather than decay towards zero and the warming from  $\text{CO}_2$  would gradually accumulate (e.g., Berntsen and Fuglestedt, 2008). The impact of contrail cirrus may even increase if emissions are kept constant while fuel efficiency is improved. The temporal behavior of total net temperature response, as well as the net  $\text{NO}_x$  effect, would differ notably from the pulse emission case.

### 3.4 Evaluation

Several studies have calculated ARTPs for emissions from specific sectors or regions (Collins et al., 2013; Lund et al.,

2014; Sand et al., 2016; Stohl et al., 2015). Stohl et al. (2015) also compared the estimated regional temperature responses to short-lived climate pollutants with those simulated by several climate models. However, these studies focus only on surface sources and the evaluation may not be valid for aviation. The regional climate sensitivities that form the basis for the ARTP calculations are derived from simulations with only one climate model. Moreover, the sensitivities are representative of the response to a vertical forcing profile resulting from total anthropogenic emissions, i.e., one that in many regions differ considerably from those induced by the mainly high-altitude aviation emissions. Several recent studies have found a strong vertical sensitivity in the BC forcing–response relationship, with decreasing efficacy with altitude (Ban-Weiss et al., 2011; Flanner, 2013; Samset and Myhre, 2015). Climate model studies also indicate that the forcing–response relationship for ozone will be dependent on both the vertical and horizontal distribution of the ozone change (Berntsen et al., 1997; Hansen et al., 1997; Joshi et al., 2003), which in turn also depends on altitude (e.g., Olsen et al., 2013). As discussed in Sect. 2.2, a formal quantification of uncertainties in the regional climate sensitivities is currently not possible. However, in light of the potential uncertainties arising from the vertical dependence, we perform a first evaluation of the ARTP concept in the context of aviation ozone and BC (Sect. 2.3). Further evaluation, especially of contrail cirrus, would be valuable but require resources beyond those available for the current study.

Figure 4a shows the normalized regional temperature response to aviation ozone, as simulated by the CESM1.2, HadSM3 and ECHAM and estimated using the regional climate sensitivities that form the basis for the ARTP concept. There are several factors potentially contributing to differences in the absolute magnitude of temperature responses in the simulations, including differences in the ozone concentration perturbation resulting from differences in emissions or ozone change per unit emission, radiative efficiency and ECS. HadSM3 and ECHAM used the multi-model average ozone concentration change resulting from year 2000 aviation  $\text{NO}_x$  emission (0.67 TgN) (Hoor et al., 2009), while this study (using CESM2.1) uses the ozone change simulated by one model (OsloCTM3) and year 2006 aviation emissions (0.81 TgN). Based on visual inspection, these two aviation-induced ozone concentration perturbations are quite similar, with slightly larger perturbation at high northern latitudes in the present study. Nonetheless, here we focus on the spatial pattern across latitude bands rather than absolute magnitudes and therefore normalize the temperature response in each band by the respective global-mean response.

The climate models and ARTP-derived estimates agree reasonably well in the 28° S–28° N and 28–60° N latitude bands. However, in both the 90–28° S and 60–90° N regions, the temperature response simulated directly by the climate models is considerably higher than that estimated using the ARTP. The low ARTP-derived temperature response in the

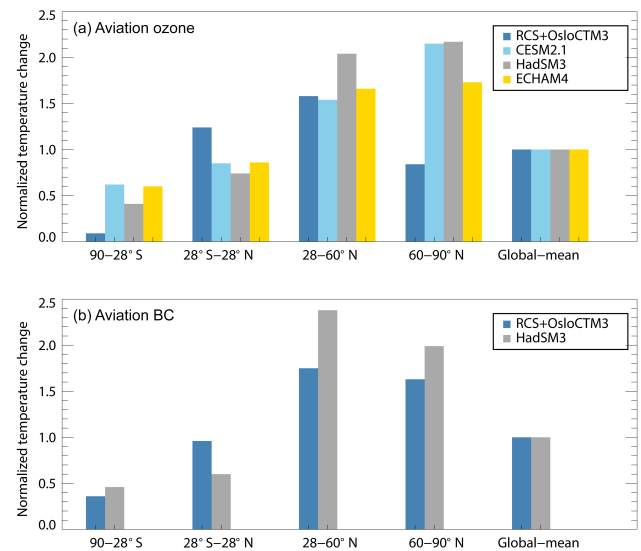


**Figure 4.** (a) Comparison of the regional pattern of surface temperature response to a global aviation ozone perturbation as calculated using the regional climate sensitivities (RCS) from GISS with RF derived from OsloCTM3 (i.e., using the ARTP concept) and simulated by HadSM3, ECHAM4 and CESM1.2. Surface temperature response in each latitude band is normalized by the global-mean value. (b) Same as (a) but for BC.

60–90° N region reflects the low sensitivity in the GISS model in this latitude band to ozone forcing exerted both locally, as well as in the 28–60° N region, where the aviation-induced forcing is highest (Fig. 1 of Shindell and Faluvegi, 2009). A low, and even negative, sensitivity to Northern Hemisphere forcing also characterizes the 90–28° S band.

The reason for the low sensitivity in the GISS simulations, or whether this is a feature specific to this model, is not clear. It is possible that the differences between modeled and estimated temperature response to aviation ozone forcing can be at least partly explained by vertical variations in the response to ozone perturbations. Early work by Hansen et al. (1997) suggested a surface cooling in response to a global near surface ozone perturbation and a maximum efficacy around 700–800 hPa, followed by a decreasing efficacy for ozone perturbations in the upper troposphere. The latter was supported by Joshi et al. (2003). However, the increased sensitivity to lower stratosphere perturbations found by Joshi et al. (2003) was not seen in the Hansen et al. (1997) results. Such uncertainties in the efficacy around the upper troposphere–lower stratosphere region are important in the case of aviation.

Figure 4b compares aviation BC temperature response to that obtained from the HadSM3. The regional distribution across latitude bands is similar for the estimated and simulated temperature response. However, here we only have temperature response simulated by one climate model. Given the substantial uncertainty and inter-model differences in model

estimates of BC climate impacts (Baker et al., 2015; Samset et al., 2014; Stohl et al., 2015), additional model simulations are needed for further comparison and evaluation.

The notable decrease in BC efficacy with altitude globally, and particularly at high latitudes (Ban-Weiss et al., 2011; Flanner, 2013; Samset and Myhre, 2015), raises the question of whether using the ARTP to estimate temperature responses to the high-altitude aviation BC forcing could result in an overestimation of the absolute magnitude. Flanner (2013) provided vertically resolved climate sensitivities for the Arctic temperature response to local Arctic BC forcing. Using these, Lund et al. (2014) found important differences in the temperature response to BC from on-road transportation in the 60–90° N latitude band compared to using the single regional climate sensitivity derived from Shindell and Faluvegi (2009) (and used in the present analysis). At the altitudes in the 60–90° N region, where the aviation-induced RF peaks, the regional climate sensitivity from Flanner (2013) and Shindell and Faluvegi (2009), and hence the estimated temperature response, agree quite well. This agreement may not hold for all regions, but similar vertically resolved climate sensitivities for other latitude bands or species do not currently exist.

Based on our analysis, some care is needed when using the ARTP with the currently available regional climate sensitivities in the context of aviation emissions. Specifically, our findings suggest that the temperature response in the 90–28° S and 60–90° N regions to aviation ozone could be underestimated. Furthermore, a possible overestimation of temperature response to aviation BC can not be ruled out. Further work to quantify the importance of vertical variations in forcing–response relationships and develop regional climate sensitivities based on vertically resolved forcing perturbations would be valuable for future use of the ARTP.

#### 4 Conclusions

We have examined the impacts of aviation emissions on global and regional temperature, characterizing them using emission metrics. We address the impacts of NO<sub>x</sub> on ozone and methane, aerosols and contrail-cirrus formation, and consider six emission regions spanning both hemispheres. In addition to updated emission metrics for global aviation, we present GWPs and GTPs on 20- and 100-year time horizons for a larger set of species and regions than previous studies. We also calculate the absolute regional temperature change potential (ARTP) for aviation, allowing us to not only capture how equal emissions in different regions impact global climate but also quantify the temperature impacts on a sub-global scale.

The metric values depend significantly on emission regions. In the case of aviation aerosols, we calculate the highest GWPs and GTPs for emissions in South Asia, followed by South America and Africa and the South Pacific Ocean. The

strong efficiency of emissions over our South Asian region reflects a relatively long lifetime of the aerosols here compared to other regions. Our results do not include aerosol–cloud interactions, an important limitation as recent studies suggest that aviation can potentially have strong impacts through modification of both cirrus and low-level clouds; however this contribution remains particularly uncertain. The net temperature impact over time following a pulse emission of aviation NO<sub>x</sub> is determined by the relative importance of the cooling and warming methane and ozone contributions, and is very sensitive to the choice of time horizon. The net NO<sub>x</sub> ARTP is negative after 20 years and switches to a small net warming on a 100-year time horizon on global mean and in the latitude band closest to the where the emissions occur. Metrics for contrail cirrus are calculated on a per unit emission of aviation CO<sub>2</sub> basis. The GWPs and GTPs are highest for North America and Europe, where contrail-cirrus formation is prevalent. However, once formed, contrail cirrus in the tropics have much higher optical depth due to the larger amount of water vapor. The metric values do not account for a lower efficacy of contrail cirrus that has been suggested by previous studies, but remains highly uncertain. Moreover, the contrail-cirrus metrics would not be appropriate if there are significant changes in routes and flight altitudes, or if changes in climate or propulsion efficiency affect the potential for contrail-cirrus formation.

The ARTPs illustrate how the latitudinal temperature pattern can differ significantly from the global-mean, as well as from the latitudinal pattern of RF. Due to the short lifetime of many of the aviation forcing mechanisms, the RF is typically largely confined to the latitude band closest to where the emissions occur. However, in a given latitude band, the temperature response can be considerably stronger than suggested by the corresponding forcing, emphasizing the importance of both forcing exerted locally and remote impacts through large-scale circulation changes and feedbacks in the climate system.

While the strongest temperature change per unit aerosol and NO<sub>x</sub> emitted is found for aviation over the South Asian region in our study, the majority of flights today take place over the northern midlatitudes. The net warming impact 20 and 100 years following a 1-year pulse emission from the present-day aviation sector is therefore largest in all latitude bands for emissions in North America and Europe, with the largest single warming contribution after 20 years from contrail cirrus. Furthermore, the effect of contrail cirrus remain notable in several regions even on a time horizon of 100 years, causing a warming impact of around 15 % of contributions from aviation CO<sub>2</sub>. The discussion around CO<sub>2</sub> often focuses on its long-term impacts. However, our results illustrate that while CO<sub>2</sub> is dominant on longer timescales, it also gives a considerable warming contribution already after 20 years. Our metric framework can also be applied to estimate regional temperature changes following more realistic emissions scenarios for the sector, which would influence the



temporal characteristic of the response and the relative contributions of short and long-lived species over time.

While the ARTP concept is an important and useful tool for providing first-order estimates of regional temperature of various emissions, our analysis indicates that some care is needed when it is used in the context of aviation emissions or, more generally, in situations that differ significantly from those used to derive the regional climate sensitivities for the ARTP calculations in the first place. In particular, further work to quantify and account for the relationship between vertically resolved radiative forcing perturbations and surface temperature response is needed to allow for more general applicability of the concept.

**Data availability.** For official inquiries related to the use of the AEDT aviation emission inventory and access to inventory files, please contact Rangasayi Halthore (Federal Aviation Administration) (rangasayi.halthore@faa.gov) and Sathya Balasubramanian (Volpe Center) (sathya.balasubramanian.CTR@dot.gov). For model results, please contact Mairanne T. Lund (CICERO) (m.t.lund@cicero.oslo.no).

**The Supplement related to this article is available online at <https://doi.org/10.5194/esd-8-547-2017-supplement>.**

**Competing interests.** The authors declare that they have no conflict of interest.

**Acknowledgements.** This is work funded by the US Federal Aviation Administration (FAA)/Volpe Center under the contract no. DTRT57-12-P-80123. We thank Øivind Hodnebrog (CICERO) for contributions.

Edited by: Ben Kravitz

Reviewed by: two anonymous referees

## References

- Aamaas, B., Peters, G. P., and Fuglestedt J. S.: Simple emission metrics for climate impacts, *Earth Syst. Dynam.*, 4, 145–170, <https://doi.org/10.5194/esd-4-145-2013>, 2013.
- Aamaas, B., Berntsen, T. K., Fuglestedt, J. S., Shine, K. P., and Bellouin, N.: Regional emission metrics for short-lived climate forcers from multiple models, *Atmos. Chem. Phys.*, 16, 7451–7468, <https://doi.org/10.5194/acp-16-7451-2016>, 2016.
- Baker, L. H., Collins, W. J., Oliv  , D. J. L., Cherian, R., Hodnebrog,  ., Myhre, G., and Quaas, J.: Climate responses to anthropogenic emissions of short-lived climate pollutants, *Atmos. Chem. Phys.*, 15, 8201–8216, <https://doi.org/10.5194/acp-15-8201-2015>, 2015.
- Ban-Weiss, G., Cao, L., Bala, G., and Caldeira, K.: Dependence of climate forcing and response on the altitude of black carbon aerosols, *Clim. Dynam.*, 38, 897–911, <https://doi.org/10.1007/s00382-011-1052-y>, 2011.
- Barrett, S., Prather, M., Penner, J., Selkirk, H., Balasubramanian, S., Doppelheuer, A., Fleming, G., Gupta, M., Halthore, R. N., Hileman, J., Jacobson, M., Kuhn, S., Lukachko, S., Miake-Lye, R., Petzold, A., Roof, C., Schaefer, M., Schumann, U., Waitz, I., and Wayson, R.: Guidance on the use of AEDT gridded aircraft emissions in atmospheric models, A technical note submitted to the US Federal Aviation Administration, Massachusetts Institute of Technology (MIT), 2010.
- Berntsen, T. K. and Fuglestedt, J.: Global temperature responses to current emissions from the transport sectors, *P. Natl. Acad. Sci. USA*, 105, 19154–19159, <https://doi.org/10.1073/pnas.0804844105>, 2008.
- Berntsen, T. K., Fuglestedt, J., Myhre, G., Stordal, F., and Berglen, T. F.: Abatement of greenhouse gases: Does location matter?, *Climatic Change*, 74, 377–411, <https://doi.org/10.1007/s10584-006-0433-4>, 2006.
- Berntsen, T. K., Isaksen, I. S. A., Myhre, G., Fuglestedt, J. S., Stordal, F., Larsen, T. A., Freckleton, R. S., and Shine, K. P.: Effects of anthropogenic emissions on tropospheric ozone and its radiative forcing, *J. Geophys. Res.-Atmos.*, 102, 28101–28126, <https://doi.org/10.1029/97JD02226>, 1997.
- Bindoff, N. L., Stott, P. A., AchutaRao, K. M., Allen, M. R., Gillett, N., Gutzler, D., Hansingo, K., Hegerl, G., Hu, Y., Jain, S., Mokhov, I. I., Overland, J., Perlwitz, J., Sebbari, R., and Zhang, X.: Detection and Attribution of Climate Change: from Global and Regional, in: *Climate Change 2013: The Physical Science Basis, Contribution of Working Group I to the Fifth Assessment Report of the Intergovernmental Panel on Climate Change*, edited by: Stocker, T. F., Qin, D., Plattner, G.-K., Tignor, M., Allen, S. K., Boschung, J., Nauels, A., Xia, Y., Bex, V., and Midgley, P. M., Cambridge University Press, Cambridge, UK and New York, NY, USA, 2013.
- Bock, L. and Burkhardt, U.: The temporal evolution of a long-lived contrail cirrus cluster: Simulations with a global climate model, *J. Geophys. Res.-Atmos.*, 121, 3548–3565, <https://doi.org/10.1002/2015JD024475>, 2016a.
- Bock, L. and Burkhardt, U.: Reassessing properties and radiative forcing of contrail cirrus using a climate model, *J. Geophys. Res.-Atmos.*, 121, 9717–9736, <https://doi.org/10.1002/2016JD025112>, 2016b.
- Boer, G. J. and Yu, B.: Climate sensitivity and response, *Clim. Dynam.*, 20, 415–429, <https://doi.org/10.1007/s00382-002-0283-3>, 2003.
- Boucher, O. and Reddy, M. S.: Climate trade-off between black carbon and carbon dioxide emissions, *Energy Policy*, 36, 193–200, <https://doi.org/10.1016/j.enpol.2007.08.039>, 2008.
- Brasseur, G. P., Gupta, M., Anderson, B. E., Balasubramanian, S., Barrett, S., Duda, D., Fleming, G., Forster, P. M., Fuglestedt, J., Gettelman, A., Halthore, R. N., Jacob, S. D., Jacobson, M. Z., Khodayari, A., Liou, K.-N., Lund, M. T., Miake-Lye, R. C., Minnis, P., Olsen, S., Penner, J. E., Prinn, R., Schumann, U., Selkirk, H. B., Sokolov, A., Unger, N., Wolfe, P., Wong, H.-W., Wuebbles, D. W., Yi, B., Yang, P., and Zhou, C.: Impact of Aviation on Climate: FAA’s Aviation Climate Change Research Ini-

- tiative (ACCRI) Phase II, *B. Am. Meteorol. Soc.*, 97, 561–583, <https://doi.org/10.1175/bams-d-13-00089.1>, 2016.
- Burkhardt, U. and Kaercher, B.: Global radiative forcing from contrail cirrus, *Nat. Clim. Change*, 1, 54–58, <https://doi.org/10.1038/nclimate1068>, 2011.
- Burkhardt, U., Kärcher, B., Ponater, M., Gierens, K., and Gettelman, A.: Contrail cirrus supporting areas in model and observations, *Geophys. Res. Lett.*, 35, L16808, <https://doi.org/10.1029/2008GL034056>, 2008.
- Collins, W. J., Fry, M. M., Yu, H., Fuglestedt, J. S., Shindell, D. T., and West, J. J.: Global and regional temperature-change potentials for near-term climate forcers, *Atmos. Chem. Phys.*, 13, 2471–2485, <https://doi.org/10.5194/acp-13-2471-2013>, 2013.
- Fahey, D. W., Keim, E. R., Boering, K. A., Brock, C. A., Wilson, J. C., Jonsson, H. H., Anthony, S., Hanisco, T. F., Wennberg, P. O., Miale-Lye, R. C., Salawitch, R. J., Louisnard, N., Woodbridge, E. L., Gao, R. S., Donnelly, S. G., Wamsley, R. C., Del Negro, L. A., Solomon, S., Daube, B. C., Wofsy, S. C., Webster, C. R., May, R. D., Kelly, K. K., Loewenstein, M., Podolske, J. R., and Chan, K. R.: Emission Measurements of the Concorde Supersonic Aircraft in the Lower Stratosphere, *Science*, 270, 70–74, <https://doi.org/10.1126/science.270.5233.70>, 1995.
- Flanner, M. G.: Arctic climate sensitivity to local black carbon, *J. Geophys. Res.-Atmos.*, 118, 1840–1851, <https://doi.org/10.1002/jgrd.50176>, 2013.
- Fry, M. M., Naik, V., West, J. J., Schwarzkopf, M. D., Fiore, A. M., Collins, W. J., Dentener, F. J., Shindell, D. T., Atherton, C., Bergmann, D., Duncan, B. N., Hess, P., MacKenzie, I. A., Marmer, E., Schultz, M. G., Szopa, S., Wild, O., and Zeng, G.: The influence of ozone precursor emissions from four world regions on tropospheric composition and radiative climate forcing, *J. Geophys. Res.-Atmos.*, 117, D07306, <https://doi.org/10.1029/2011jd017134>, 2012.
- Fuglestedt, J. S., Berntsen, T. K., Godal, O., Sausen, R., Shine, K. P., and Skodvin, T.: Metrics of climate change: Assessing radiative forcing and emission indices, *Climatic Change*, 58, 267–331, 2003.
- Fuglestedt, J. S., Shine, K. P., Berntsen, T., Cook, J., Lee, D. S., Stenke, A., Skeie, R. B., Velders, G. J. M., and Waitz, I. A.: Transport impacts on atmosphere and climate: Metrics, *Atmos. Environ.*, 44, 4648–4677, <https://doi.org/10.1016/j.atmosenv.2009.04.044>, 2010.
- Gasser, T., Peters, G. P., Fuglestedt, J. S., Collins, W. J., Shindell, D. T., and Ciais, P.: Accounting for the climate–carbon feedback in emission metrics, *Earth Syst. Dynam.*, 8, 235–253, <https://doi.org/10.5194/esd-8-235-2017>, 2017.
- Gettelman, A. and Chen, C.: The climate impact of aviation aerosols, *Geophys. Res. Lett.*, 40, 2785–2789, <https://doi.org/10.1002/grl.50520>, 2013.
- Gilmore, C. K., Barrett, S. R. H., Koo, J., and Wang, Q.: Temporal and spatial variability in the aviation  $\text{NO}_x$ -related  $\text{O}_3$  impact, *Environ. Res. Lett.*, 8, 034027, <https://doi.org/10.1088/1748-9326/8/3/034027>, 2013.
- Hansen, J., Sato, M., and Ruedy, R.: Radiative forcing and climate response, *J. Geophys. Res.-Atmos.*, 102, 6831–6864, <https://doi.org/10.1029/96JD03436>, 1997.
- Hansen, J., Sato, M., Ruedy, R., Nazarenko, L., Lacis, A., Schmidt, G. A., Russell, G., Aleinov, I., Bauer, M., Bauer, S., Bell, N., Cairns, B., Canuto, V., Chandler, M., Cheng, Y., Del Genio, A., Faluvegi, G., Fleming, E., Friend, A., Hall, T., Jackman, C., Kelley, M., Kiang, N., Koch, D., Lean, J., Lerner, J., Lo, K., Menon, S., Miller, R., Minnis, P., Novakov, T., Oinas, V., Perlwitz, J., Rind, D., Romanou, A., Shindell, D., Stone, P., Sun, S., Tausnev, N., Thresher, D., Wielicki, B., Wong, T., Yao, M., and Zhang, S.: Efficacy of climate forcings, *J. Geophys. Res.-Atmos.*, 110, D18104, <https://doi.org/10.1029/2005jd005776>, 2005.
- Holmes, C. D., Prather, M. J., Sovde, O. A., and Myhre, G.: Future methane, hydroxyl, and their uncertainties: key climate and emission parameters for future predictions, *Atmos. Chem. Phys.*, 13, 285–302, <https://doi.org/10.5194/acp-13-285-2013>, 2013.
- Hoor, P., Borken-Kleefeld, J., Caro, D., Dessens, O., Endresen, O., Gauss, M., Grewe, V., Hauglustaine, D., Isaksen, I. S. A., Jäckel, P., Lelieveld, J., Myhre, G., Meijer, E., Olivie, D., Prather, M., Schnadt Poberaj, C., Shine, K. P., Staehelin, J., Tang, Q., van Aardenne, J., van Velthoven, P., and Sausen, R.: The impact of traffic emissions on atmospheric ozone and OH: results from QUANTIFY, *Atmos. Chem. Phys.*, 9, 3113–3136, <https://doi.org/10.5194/acp-9-3113-2009>, 2009.
- Hurrell, J. W., Holland, M. M., Gent, P. R., Ghan, S., Kay, J. E., Kushner, P. J., Lamarque, J.-F., Large, W. G., Lawrence, D., Lindsay, K., Lipscomb, W. H., Long, M. C., Mahowald, N., Marsh, D. R., Neale, R. B., Rasch, P., Vavrus, S., Vertenstein, M., Bader, D., Collins, W. D., Hack, J. J., Kiehl, J., and Marshall, S.: The Community Earth System Model: A Framework for Collaborative Research, *B. Am. Meteorol. Soc.*, 94, 1339–1360, <https://doi.org/10.1175/BAMS-D-12-00121.1>, 2013.
- Huszar, P., Teyssèdre, H., Michou, M., Voldoire, A., Olivie, D. J. L., Saint-Martin, D., Cariolle, D., Senesi, S., Salas Y Melia, D., Alias, A., Karcher, F., Ricaud, P., and Halenka, T.: Modeling the present and future impact of aviation on climate: an AOGCM approach with online coupled chemistry, *Atmos. Chem. Phys.*, 13, 10027–10048, <https://doi.org/10.5194/acp-13-10027-2013>, 2013.
- IPCC: Climate Change 2013: The Physical Science Basis, in: Contribution of Working Group I to the Fifth Assessment Report of the Intergovernmental Panel on Climate Change, edited by: Stocker, T. F., Qin, D., Plattner, G.-K., Tignor, M., Allen, S. K., Boschung, J., Nauels, A., Xia, Y., Bex, V., and Midgley, P. M., Cambridge University Press, Cambridge, UK and New York, NY, USA, 1535 pp., 2014.
- Irvine, E. A. and Shine, K. P.: Ice supersaturation and the potential for contrail formation in a changing climate, *Earth Syst. Dynam.*, 6, 555–568, <https://doi.org/10.5194/esd-6-555-2015>, 2015.
- Jacobson, M. Z., Wilkerson, J. T., Balasubramanian, S., Cooper Jr., W. W., and Mohleji, N.: The effects of rerouting aircraft around the arctic circle on arctic and global climate, *Climatic Change*, 115, 709–724, <https://doi.org/10.1007/s10584-012-0462-0>, 2012.
- Janssens-Maenhout, G., Crippa, M., Guizzardi, D., Dentener, F., Muntean, M., Pouliot, G., Keating, T., Zhang, Q., Kurokawa, J., Wankmüller, R., Denier van der Gon, H., Kuenen, J. J. P., Klimont, Z., Frost, G., Darras, S., Koffi, B., and Li, M.: HTAP\_v2.2: a mosaic of regional and global emission grid maps for 2008 and 2010 to study hemispheric transport of air pollution, *Atmos. Chem. Phys.*, 15, 11411–11432, <https://doi.org/10.5194/acp-15-11411-2015>, 2015.
- Joos, F., Roth, R., Fuglestedt, J. S., Peters, G. P., Enting, I. G., von Bloh, W., Brovkin, V., Burke, E. J., Eby, M., Edwards, N.

- R., Friedrich, T., Frölicher, T. L., Halloran, P. R., Holden, P. B., Jones, C., Kleinen, T., Mackenzie, F. T., Matsumoto, K., Meinshausen, M., Plattner, G.-K., Reisinger, A., Segschneider, J., Shaffer, G., Steinacher, M., Strassmann, K., Tanaka, K., Timmermann, A., and Weaver, A. J.: Carbon dioxide and climate impulse response functions for the computation of greenhouse gas metrics: a multi-model analysis, *Atmos. Chem. Phys.*, 13, 2793–2825, <https://doi.org/10.5194/acp-13-2793-2013>, 2013.
- Joshi, M., Shine, K., Ponater, M., Stuber, N., Sausen, R., and Li, L.: A comparison of climate response to different radiative forcings in three general circulation models: towards an improved metric of climate change, *Clim. Dynam.*, 20, 843–854, <https://doi.org/10.1007/s00382-003-0305-9>, 2003.
- Kapadia, Z. Z., Spracklen, D. V., Arnold, S. R., Borman, D. J., Mann, G. W., Pringle, K. J., Monks, S. A., Reddington, C. L., Benduhn, F., Rap, A., Scott, C. E., Butt, E. W., and Yoshioka, M.: Impacts of aviation fuel sulfur content on climate and human health, *Atmos. Chem. Phys.*, 16, 10521–10541, <https://doi.org/10.5194/acp-16-10521-2016>, 2016.
- Khodayari, A., Wuebbles, D. J., Olsen, S. C., Fuglestedt, J. S., Berntsen, T., Lund, M. T., Waitz, I., Wolfe, P., Forster, P. M., Meinshausen, M., Lee, D. S., and Lim, L. L.: Intercomparison of the capabilities of simplified climate models to project the effects of aviation CO<sub>2</sub> on climate, *Atmos. Environ.*, 75, 321–328, <https://doi.org/10.1016/j.atmosenv.2013.03.055>, 2013.
- Köhler, M. O., Radel, G., Shine, K. P., Rogers, H. L., and Pyle, J. A.: (2013). Latitudinal variation of the effect of aviation NO<sub>x</sub> emissions on atmospheric ozone and methane and related climate metrics, *Atmos. Environ.*, 64, 1–9, <https://doi.org/10.1016/j.atmosenv.2012.09.013>, 2013.
- Lamquin, N., Stubenrauch, C. J., Gierens, K., Burkhardt, U., and Smit, H.: A global climatology of upper-tropospheric ice supersaturation occurrence inferred from the Atmospheric Infrared Sounder calibrated by MOZIC, *Atmos. Chem. Phys.*, 12, 381–405, <https://doi.org/10.5194/acp-12-381-2012>, 2012.
- Lee, D. S., Fahey, D. W., Forster, P. M., Newton, P. J., Wit, R. C. N., Lim, L. L., Owen, B., and Sausen, R.: Aviation and global climate change in the 21st century, *Atmos. Environ.*, 43, 3520–3537, <https://doi.org/10.1016/j.atmosenv.2009.04.024>, 2009.
- Lund, M. T., Berntsen, T., Fuglestedt, J. S., Ponater, M., and Shine, K. P.: How much information is lost by using global-mean climate metrics? an example using the transport sector, *Climatic Change*, 113, 949–963, <https://doi.org/10.1007/s10584-011-0391-3>, 2012.
- Lund, M. T., Berntsen, T. K., Heyes, C., Klimont, Z., Samset, B. H.: Global and regional climate impacts of black carbon and co-emitted species from the on-road diesel sector, *Atmos. Environ.*, 98, 50–58, <https://doi.org/10.1016/j.atmosenv.2014.08.033>, 2014.
- Marais, K., Lukachko, S. P., Jun, M., Mahashabde, A., and Waitz, I. A.: Assessing the impact of aviation on climate, *Meteorol. Z.*, 17, 157–172, <https://doi.org/10.1127/0941-2948/2008/0274>, 2008.
- Myhre, G., Karlsdóttir, S., Isaksen, I. S. A., and Stordal, F.: Radiative forcing due to changes in tropospheric ozone in the period 1980 to 1998, *J. Geophys. Res.*, 105, 28935–28942, <https://doi.org/10.1029/2000JD900187>, 2000.
- Myhre, G., Nilsen, J. S., Gulstad, L., Shine, K. P., Rognerud, B., and Isaksen, I. S. A.: Radiative forcing due to stratospheric water vapour from CH<sub>4</sub> oxidation, *Geophys. Res. Lett.*, 34, L01807, <https://doi.org/10.1029/2006GL027472>, 2007.
- Myhre, G., Shine, K. P., Radel, G., Gauss, M., Isaksen, I. S. A., Tang, Q., Prather, M. J., Williams, J. E., van Velthoven, P., Dessens, O., Koffi, B., Szopa, S., Hoor, P., Grewe, V., Borken-Kleefeld, J., Berntsen, T. K., and Fuglestedt, J. S.: Radiative forcing due to changes in ozone and methane caused by the transport sector, *Atmos. Environ.*, 45, 387–394, <https://doi.org/10.1016/j.atmosenv.2010.10.001>, 2011.
- Myhre, G., Samset, B. H., Schulz, M., Balkanski, Y., Bauer, S., Berntsen, T. K., Bian, H., Bellouin, N., Chin, M., Diehl, T., Easter, R. C., Feichter, J., Ghan, S. J., Hauglustaine, D., Iversen, T., Kinne, S., Kirkevåg, A., Lamarque, J.-F., Lin, G., Liu, X., Lund, M. T., Luo, G., Ma, X., van Noije, T., Penner, J. E., Rasch, P. J., Ruiz, A., Seland, Ø., Skeie, R. B., Stier, P., Takemura, T., Tsigaridis, K., Wang, P., Wang, Z., Xu, L., Yu, H., Yu, F., Yoon, J.-H., Zhang, K., Zhang, H., and Zhou, C.: Radiative forcing of the direct aerosol effect from AeroCom Phase II simulations, *Atmos. Chem. Phys.*, 13, 1853–1877, <https://doi.org/10.5194/acp-13-1853-2013>, 2013a.
- Myhre, G., Shindell, D., Brèon, F.-M., Collins, W., Fuglestedt, J., Huang, J., Koch, D., Lamarque, J.-F., Lee, D., Mendoza, B., Nakajima, T., Robock, A., Stephens, G., Takemura, T., and Zhang, H.: Anthropogenic and natural radiative forcing, in: *Climate Change 2013: The Physical Science Basis. Contribution of Working Group I to the Fifth Assessment Report of the Intergovernmental Panel on Climate Change*, edited by: Stocker, T. F., Qin, D., Plattner, G.-K., Tignor, M., Allen, S. K., Boschung, J., Nauels, A., Xia, Y., Bex, V., and Midgley, P. M., Cambridge University Press, Cambridge, UK and New York, NY, USA, 2013b.
- Newinger, C. and Burkhardt, U.: Sensitivity of contrail cirrus radiative forcing to air traffic scheduling, *J. Geophys. Res.-Atmos.*, 117, D10205, <https://doi.org/10.1029/2011JD016736>, 2012.
- Olivié, D. J. L., Cariolle, D., Teyssèdre, H., Salas, D., Voldoire, A., Clark, H., Saint-Martin, D., Michou, M., Karcher, F., Balkanski, Y., Gauss, M., Dessens, O., Koffi, B., and Sausen, R.: Modeling the climate impact of road transport, maritime shipping and aviation over the period 1860–2100 with an AOGCM, *Atmos. Chem. Phys.*, 12, 1449–1480, <https://doi.org/10.5194/acp-12-1449-2012>, 2012.
- Olsen, S. C., Brasseur, G. P., Wuebbles, D. J., Barrett, S. R. H., Dang, H., Eastham, S. D., Jacobson, M. Z., Khodayari, A., Selkirk, H., Sokolov, A., and Unger, N.: Comparison of model estimates of the effects of aviation emissions on atmospheric ozone and methane, *Geophys. Res. Lett.*, 40, 6004–6009, <https://doi.org/10.1002/2013GL057660>, 2013.
- Penner, J. E., Lister, D. H., Griggs, D. J., Dokken, D. J., and McFarland, M.: *Aviation and the global atmosphere*, Cambridge Univ. Press, Cambridge, 365 pp., 1999.
- Ponater, M., Marquart, S., Sausen, R., and Schumann, U.: On contrail climate sensitivity, *Geophys. Res. Lett.*, 32, L10706, <https://doi.org/10.1029/2005GL022580>, 2005.
- Ponater, M., Dietmüller, S., Stuber, N., Shine, K. P., Highwood, E. J., and Radel, G.: Indications of distinctive efficacies for transport related ozone perturbations, paper presented at Second International Conference on Transport, Atmosphere and Climate (TAC-2), 22–25 June 2009, Aachen and Maastricht, 2009.
- Rap, A., Forster, P. M., Haywood, J. M., Jones, A., and Boucher, O.: Estimating the climate impact of linear contrails using the

- UK Met Office climate model, *Geophys. Res. Lett.*, 37, L20703, <https://doi.org/10.1029/2010GL045161>, 2010.
- Righi, M., Hendricks, J., and Sausen, R.: The global impact of the transport sectors on atmospheric aerosol in 2030 – Part 2: Aviation, *Atmos. Chem. Phys.*, 16, 4481–4495, <https://doi.org/10.5194/acp-16-4481-2016>, 2016.
- Samset, B. H. and Myhre, G.: Vertical dependence of black carbon, sulphate and biomass burning aerosol radiative forcing, *Geophys. Res. Lett.*, 38, L24802, <https://doi.org/10.1029/2011gl049697>, 2011.
- Samset, B. H. and Myhre, G.: Climate response to externally mixed black carbon as a function of altitude, *J. Geophys. Res.-Atmos.*, 120, 2913–2927, <https://doi.org/10.1002/2014JD022849>, 2015.
- Samset, B. H., Myhre, G., Herber, A., Kondo, Y., Li, S.-M., Moteki, N., Koike, M., Oshima, N., Schwarz, J. P., Balkanski, Y., Bauer, S. E., Bellouin, N., Bernsten, T. K., Bian, H., Chin, M., Diehl, T., Easter, R. C., Ghan, S. J., Iversen, T., Kirkevåg, A., Lamarque, J.-F., Lin, G., Liu, X., Penner, J. E., Schulz, M., Seland, Ø., Skeie, R. B., Stier, P., Takemura, T., Tsigaridis, K., and Zhang, K.: Modelled black carbon radiative forcing and atmospheric lifetime in AeroCom Phase II constrained by aircraft observations, *Atmos. Chem. Phys.*, 14, 12465–12477, <https://doi.org/10.5194/acp-14-12465-2014>, 2014.
- Sand, M., Bernsten, T. K., Kay, J. E., Lamarque, J. F., Seland, Ø., and Kirkevåg, A.: The Arctic response to remote and local forcing of black carbon, *Atmos. Chem. Phys.*, 13, 211–224, <https://doi.org/10.5194/acp-13-211-2013>, 2013.
- Sand, M., Bernsten, T. K., von Salzen, K., Flanner, M. G., Langner, J., and Victor, D. G.: Response of Arctic temperature to changes in emissions of short-lived climate forcers, *Nat. Clim. Change*, 6, 286–289, <https://doi.org/10.1038/nclimate2880>, 2016.
- Sausen, R., Isaksen, I., Grewe, V., Hauglustaine, D., Lee, D. S., Myhre, G., Kohler, M. O., Pitari, G., Schumann, U., Stordal, F., and Zerefos, C.: Aviation radiative forcing in 2000: An update on IPCC (1999), *Meteorol. Z.*, 14, 555–561, <https://doi.org/10.1127/0941-2948/2005/0049>, 2005.
- Schulz, M., Textor, C., Kinne, S., Balkanski, Y., Bauer, S., Bernsten, T., Berglen, T., Boucher, O., Dentener, F., Guibert, S., Isaksen, I. S. A., Iversen, T., Koch, D., Kirkevåg, A., Liu, X., Montanaro, V., Myhre, G., Penner, J. E., Pitari, G., Reddy, S., Seland, Ø., Stier, P., and Takemura, T.: Radiative forcing by aerosols as derived from the AeroCom present-day and pre-industrial simulations, *Atmos. Chem. Phys.*, 6, 5225–5246, <https://doi.org/10.5194/acp-6-5225-2006>, 2006.
- Shindell, D. and Faluvegi, G.: Climate response to regional radiative forcing during the twentieth century, *Nat. Geosci.*, 2, 294–300, <https://doi.org/10.1038/ngeo473>, 2009.
- Shindell, D. and Faluvegi, G.: The net climate impact of coal-fired power plant emissions, *Atmos. Chem. Phys.*, 10, 3247–3260, <https://doi.org/10.5194/acp-10-3247-2010>, 2010.
- Shindell, D., Schulz, M., Ming, Y., Takemura, T., Faluvegi, G., and Ramaswamy, V.: Spatial scales of climate response to inhomogeneous radiative forcing, *J. Geophys. Res.*, 115, D19110, <https://doi.org/10.1029/2010jd014108>, 2010.
- Shindell, D. T.: Evaluation of the absolute regional temperature potential, *Atmos. Chem. Phys.*, 12, 7955–7960, <https://doi.org/10.5194/acp-12-7955-2012>, 2012.
- Shine, K. P., Bernsten, T. K., Fuglestedt, J. S., and Sausen, R.: Scientific issues in the design of metrics for inclusion of oxides of nitrogen in global climate agreements, *P. Natl. Acad. Sci. USA*, 102, 15768–15773, <https://doi.org/10.1073/pnas.0506865102>, 2005a.
- Shine, K. P., Fuglestedt, J. S., Hailemariam, K., and Stuber, N.: Alternatives to the global warming potential for comparing climate impacts of emissions of greenhouse gases, *Climatic Change*, 68, 281–302, <https://doi.org/10.1007/s10584-005-1146-9>, 2005b.
- Shine, K. P., Highwood, E. J., Rädcl, G., Stuber, N., and Balkanski, Y.: Climate model calculations of the impact of aerosols from road transport and shipping, *Atmos. Ocean. Opt.*, 25, 62–70, <https://doi.org/10.1134/s1024856012010125>, 2012.
- Skeie, R. B., Fuglestedt, J., Bernsten, T., Lund, M. T., Myhre, G., and Rypdal, K.: Global temperature change from the transport sectors: Historical development and future scenarios, *Atmos. Environ.*, 43, 6260–6270, 2009.
- Skowron, A., Lee, D. S., and De León, R. R.: The assessment of the impact of aviation NO<sub>x</sub> on ozone and other radiative forcing responses – The importance of representing cruise altitudes accurately, *Atmos. Environ.*, 74, 159–168, <https://doi.org/10.1016/j.atmosenv.2013.03.034>, 2013.
- Søvde, O. A., Prather, M. J., Isaksen, I. S. A., Bernsten, T. K., Stordal, F., Zhu, X., Holmes, C. D., and Hsu, J.: The chemical transport model Oslo CTM3, *Geosci. Model Dev.*, 5, 1441–1469, <https://doi.org/10.5194/gmd-5-1441-2012>, 2012.
- Stenke, A., Grewe, V., and Ponater, M.: Lagrangian transport of water vapor and cloud water in the ECHAM4 GCM and its impact on the cold bias, *Clim. Dynam.*, 31, 491–506, <https://doi.org/10.1007/s00382-007-0347-5>, 2008.
- Stevenson, D. S. and Derwent, R. G.: Does the location of aircraft nitrogen oxide emissions affect their climate impact?, *Geophys. Res. Lett.*, 36, L17810, <https://doi.org/10.1029/2009gl039422>, 2009.
- Stohl, A., Aamaas, B., Amann, M., Baker, L. H., Bellouin, N., Bernsten, T. K., Boucher, O., Cherian, R., Collins, W., Daskalakis, N., Dusinska, M., Eckhardt, S., Fuglestedt, J. S., Harju, M., Heyes, C., Hodnebrog, Ø., Hao, J., Im, U., Kanakidou, M., Klimont, Z., Kupiainen, K., Law, K. S., Lund, M. T., Maas, R., MacIntosh, C. R., Myhre, G., Myriokefalitakis, S., Olivie, D., Quaas, J., Quennehen, B., Raut, J.-C., Rumbold, S. T., Samset, B. H., Schulz, M., Seland, Ø., Shine, K. P., Skeie, R. B., Wang, S., Yttri, K. E., and Zhu, T.: Evaluating the climate and air quality impacts of short-lived pollutants, *Atmos. Chem. Phys.*, 15, 10529–10566, <https://doi.org/10.5194/acp-15-10529-2015>, 2015.
- Stuber, N., Forster, P., Rädcl, G., and Shine, K.: The importance of the diurnal and annual cycle of air traffic for contrail radiative forcing, *Nature*, 441, 864–867, 2006.
- Unger, N., Zhao, Y., and Dang, H.: Mid-21st century chemical forcing of climate by the civil aviation sector, *Geophys. Res. Lett.*, 40, 641–645, <https://doi.org/10.1002/grl.50161>, 2013.
- van der Werf, G. R., Randerson, J. T., Giglio, L., Collatz, G. J., Mu, M., Kasibhatla, P. S., Morton, D. C., DeFries, R. S., Jin, Y., and van Leeuwen, T. T.: Global fire emissions and the contribution of deforestation, savanna, forest, agricultural, and peat fires (1997–2009), *Atmos. Chem. Phys.*, 10, 11707–11735, <https://doi.org/10.5194/acp-10-11707-2010>, 2010.
- Wild, O., Prather, M. J., and Akimoto, H.: Indirect long-term global radiative cooling from NO<sub>x</sub> Emissions, *Geophys. Res. Lett.*, 28, 1719–1722, <https://doi.org/10.1029/2000GL012573>, 2001.



- Wilkerson, J. T., Jacobson, M. Z., Malwitz, A., Balasubramanian, S., Wayson, R., Fleming, G., Naiman, A. D., and Lele, S. K.: Analysis of emission data from global commercial aviation: 2004 and 2006, *Atmos. Chem. Phys.*, 10, 6391–6408, <https://doi.org/10.5194/acp-10-6391-2010>, 2010.
- Wilks, D. S.: On “Field Significance” and the False Discovery Rate, *J. Appl. Meteorol. Clim.*, 45, 1181–1189, <https://doi.org/10.1175/JAM2404.1>, 2006.
- Williams, K. D., Senior, C. A., and Mitchell, J. F. B.: Transient climate change in the Hadley Centre models: The role of physical processes, *J. Climate*, 14, 2659–2674, 2001.
- Zhou, C. and Penner, J. E.: Aircraft soot indirect effect on large-scale cirrus clouds: Is the indirect forcing by aircraft soot positive or negative?, *J. Geophys. Res.-Atmos.*, 119, 11303–11320, <https://doi.org/10.1002/2014JD021914>, 2001.